Interference Analysis in an Urban Mesh Network Operating in the 60-GHz Band

Maryam Eslami Rasekh and Forouhar Farzaneh

Because of their exclusive features, millimeter wave directive mesh networks can be considered for small cell backhaul support in urban environments. For this purpose, a network of closely spaced stations has been considered with very directive line-of-sight links operating in the 60-GHz band. An attempt is made to evaluate channel response and interference behavior in such a network, taking into account the effect of building blockage. A simple grid of building blocks is considered as the propagation environment, and wave propagation is simulated using 2.5-dimensional (2.5D) ray tracing (2D with ground effect) to calculate the received signal at different nodes in the network. The results are compared with free space predictions and used to evaluate interference at all nodes in the channel and describe certain characteristics of links, such as the delay profile and the correlation length.

Keywords: Millimeter wave propagation, dense urban backhaul, ray tracing, directive mesh networks, interference, 60 GHz.

I. Introduction

Millimeter wave frequencies, specifically the 60-GHz band, possess distinct characteristics that set them apart from other frequency bands in many ways. Their short wavelength introduces higher path loss and severe attenuation from scattering in the propagation environment. High path loss and low available power bring about the need for directive antennas to overcome path loss even for short links. At these frequencies, high gain and small antennas are feasible and commercially available [1], and research is underway toward the development and improvement of directive steerable antennas in this band [2], [3]. Another feature of the 60-GHz band is the high unlicensed bandwidth available, which provides the potential for very high bitrates [4].

Because of these features, millimeter wave mesh networks can be considered for small cell backhaul support in urban environments as a substitute for fiber [5]. Recent trends show that cellular mobile communication is headed toward smaller cells and higher per user bitrates. Small cells means more densely located stations and thus high cost for fiber backhaul implementation. Yet, a directive mesh network operating in the unlicensed millimeter wave band (namely, 60 GHz) can provide all that we are looking for: small cells with short links, high data rate (due to huge available spectrum), low cost (no licensing cost), and robust implementation (small antennas with high gain). Over all, free spectrum licensing and elimination of the need for costly trenching and fiber installation along with speedy, robust deployment give the wireless mesh backhaul option a considerable advantage over fiber [5], [6].

In such a network, each mesh point provides an access point for users in its proximity. We shall refer to the area supported

Manuscript received Oct. 27, 2012; revised Jan. 7, 2013; accepted Jan. 21, 2013.

This work was supported by Iran Telecommunications Research Center, Tehran, Iran (T/19253/500).

Maryam Eslami Rasekh (phone: +98 21 6616 5948, erasekh@ee.sharif.edu) and Forouhar Farzaneh (farzaneh@sharif.edu) are with the School of Electrical Engineering, Sharif University of Technology, Tehran, Iran.

http://dx.doi.org/10.4218/etrij.13.0112.0736

by an access point as its cell. Each backhaul mesh station is located close to an access point (on the same mount if possible) and delivers the data load of the users in its cell to and from the core network. A major distinction of such a network is the placement of station antennas. Normally in a cellular network, base station antennas are mounted as high as possible to extend the reach of the station. Yet, in a small cell structure with cell radii as small as a few tens of meters, access point antennas must be located at lower heights to limit inter-cell interference and limit cell boundaries. Here, we consider a network of nodes in a simplified approximation for an urban environment consisting of city blocks and streets with nodes located at street crossings and antenna heights below rooftop level.

Such a network is very different from existing directive networks, and the models and methods available are not suitable for a millimeter wave mesh. High frequency rays are more severely attenuated by such propagation phenomena as diffraction, scattering, and reflection from rough surfaces, so 60-GHz signals exhibit a lower multipath power level and less penetration in faraway areas without a clear line of sight (LOS) to the transmitter (TX). The high gain of 60-GHz antennas (over 20 dB [1]) provides a high level of spatial isolation between links and opportunity for vigorous spatial reuse, unlike directive networks at lower frequencies. Therefore, extensive study and evaluation is required for the design of such a network.

Most of the previous work on outdoor directive networks thus far has concentrated on lower frequency bands utilizing both directional and omnidirectional transmission [7]-[14]. Such an approach is not suitable here because of the higher directivity of millimeter wave antennas and unfeasibility of omnidirectional transmission. Other attempts, such as in [15], have addressed the problem of interference modeling and link scheduling in a directive mesh network; yet, in these attempts, directivities were small and antennas were assumed to exist in free space (FS) with no blockage or propagation mechanisms involved.

After the 60-GHz band became available for unlicensed use in 2001, it attracted a great amount of attention. Due to severe oxygen absorption (as high as 15 dB/km), most of the recent work has been on indoor applications of 60-GHz communication [16]-[23]. However, outdoor applications that make use of the distinct characteristics of the 60-GHz band have also been considered [24], [25]. While most of the work on outdoor 60-GHz networks has neglected the problem of interference between links and focused on matters such as antenna alignment, neighbor discovery, and the problem of deafness, an attempt has been made to evaluate interference behavior in an outdoor millimeter wave mesh with directive antennas in [26]. Here, we add the effect of building blockage to assess the impact of the propagation environment on interference shaping when antennas are placed below rooftop level. Wave propagation is simulated using ray tracing, and the received signal at different nodes in the network is used to evaluate channel response at the designated receiver (RX) and interference at other nodes in the network.

In section II, the simulation procedure is explained. The results are presented and discussed in section III, followed by conclusions and suggestions of areas for further study in section IV.

II. Simulation Scenario

In many of the previous attempts to model interference for outdoor directive mesh networks at 60 GHz, structures and obstacles in the environment were neglected [26]. This would be more or less acceptable if the antennas were above rooftop level with small vertical beamwidths, but this FS assumption is not very accurate in a scenario in which nodes are beneath rooftop level. In such a case, blockage and wave guiding caused by building blocks could greatly affect the interference behavior of the network.

To understand how stations interfere with each other in the implementation described in the previous section, we need some sense of the topology of the network. For easy implementation, mesh nodes should be placed close to access points of the small cell network, that is, on the same mount. So, the location of our mesh nodes is defined by the location of the cell centers. Stations with short ranges should be located close to the ground, beneath rooftop level. To increase the reach of a station to nearby areas, it is best to locate the station at a crossroad rather than in the middle of a street block. This way, the number of stations required to provide coverage for a given area is minimized (Fig. 1).

We considered a 1,740 m × 2,180 m area of a hypothetical

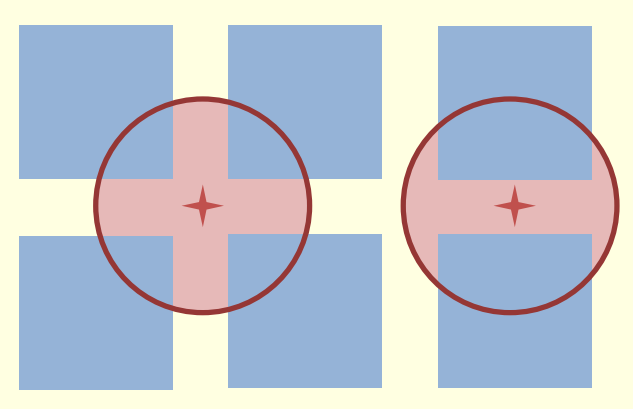

Fig. 1. Cell coverage with node at intersection and node at middle point of block.

city consisting of an 8×10 grid of square blocks, each 200 m wide and having 20 m of space between them (Fig. 2). This arrangement produces streets that are 20 m wide and 200 m long.

Figure 3 shows a real world scenario and how it might fit in the proposed model. This figure shows a 1,000 m × 600 m portion of the city of Ottawa, Ontario, Canada, as shown in [27], fitted into a grid of building blocks with widths ranging from 150 m to 200 m. This same map was used in previous work [28] to analyze and evaluate the ray tracing code used by comparing the results to the measurements in [27]. The ray tracing code used here is evaluated by comparing the results to the measurements reported in [29], showing agreement [30].

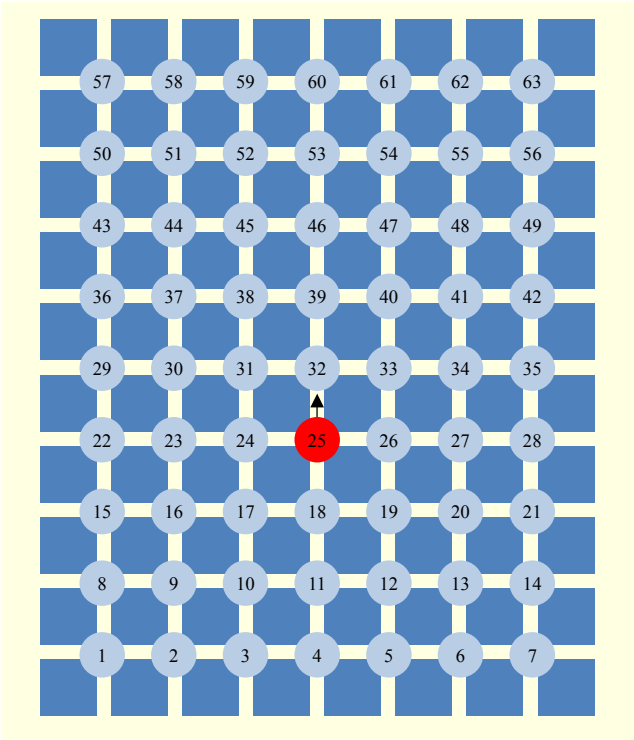

Fig. 2. Simulation scenario and station numbering.

It is worth noting that the deviation of our simplified map from reality is slight because we showed in [31] that a real city street can be approximated with great accuracy with a simple canyon guiding LOS and reflected components to the RX, even with wide irregularities and breaks (due to the intersections) in the street walls. Figure 4 shows a comparison of ray tracing results in the actual map and a simple street canyon approximation.

In our proposed scenario, the walls are assumed to be made of concrete with a relative permittivity of 7, and the permittivity of the ground is assumed to be 15. A conductivity of 0.2 and 0.05 is considered for the walls and ground, respectively [27]. Stations are placed at street intersections with each node connected to the nodes at its four neighboring intersections using a 60-GHz wireless link. Because of the symmetry of this scenario, we can infer that the amount of interference of one transmitting link accurately indicates the amount of interference of all the other links in the network. Figure 2 shows the proposed map. Nodes are numbered for referencing. Node 25 transmits on its northward link, and the received power is computed at the receiving end of each link, that is, at the north-, east-, south-, and west-facing antennas of every node.

Antennas are placed at a height of 3 m, and the heights of the surrounding buildings are thought to be much greater than the TX and RX antennas; therefore, diffraction over buildings can be ignored and 2.5D ray tracing can be considered an acceptable approximation. A total of 3,600 rays with uniform angular spacing are emitted from the TX and traced through

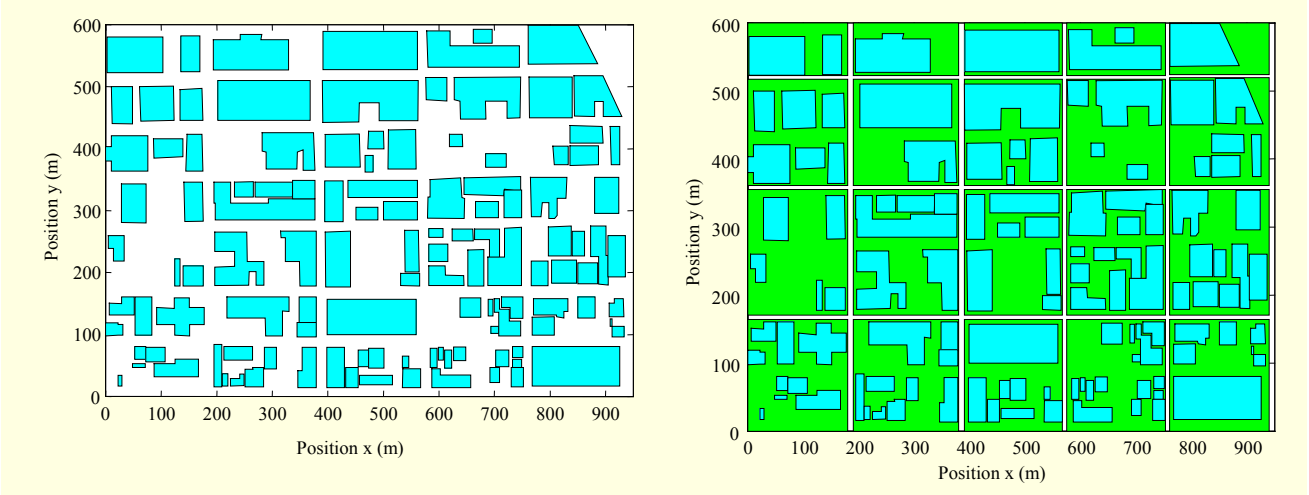

Fig. 3. Fitting real structure of part of city of Ottawa to simple block model.

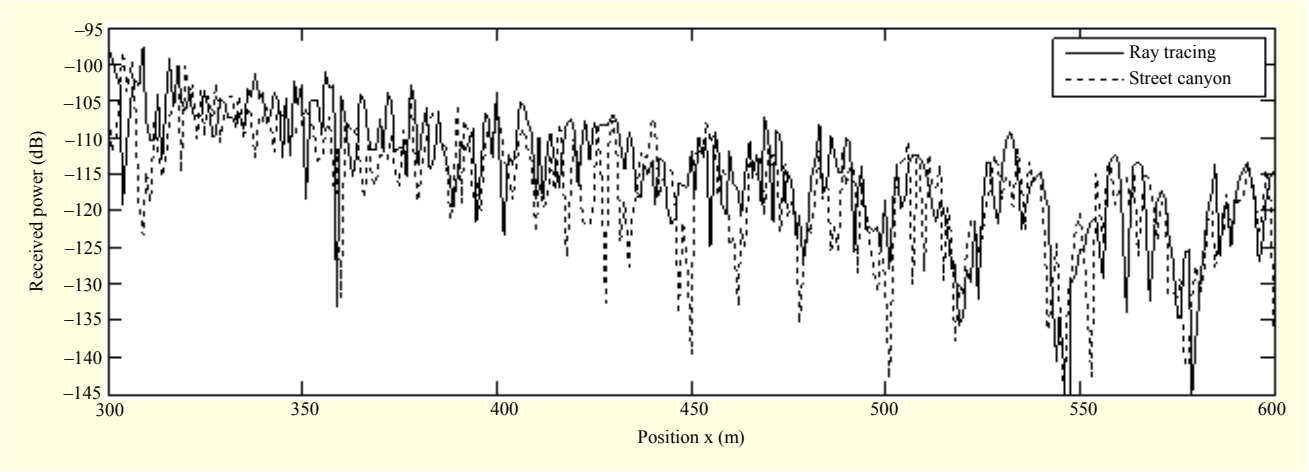

Fig. 4. Comparison of results of ray tracing on real city map and predictions of simple street canyon model.

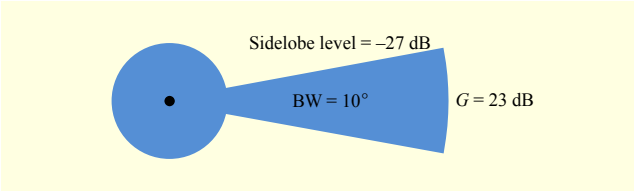

Fig. 5. Antenna pattern and characteristics.

the city until they either leave the map or die down to a level corresponding to 10 km of FS propagation. Rays that hit building corners are assumed to be diffracted in all directions with the diffraction loss of each direction calculated using the uniform theory of diffraction [32]. In other words, the building corner is modeled as a new origin of radiation emitting up to 360 new rays with a uniform angular spacing of 1 degree. The chosen degree of angular spacing of the diffracted rays cannot be very small because it has an exponential effect on the program runtime. Rays are traced in two dimensions; for each path connecting the TX to a receiving point, the corresponding ground-reflected path is added to the received components, thus turning the simulation into a 2.5D simulation.

Transmitting and receiving antennas are modeled as perfect sector antennas, the properties of which are described in Fig. 5. The main beam has a 23-dB gain and an angular width of 10 degrees. A uniform sidelobe with a −27-dB gain relative to the main beam is considered outside the main beam.

As shown in Fig. 2, due to the symmetry of the scenario, nearly half the points can be ignored (the nodes on the left and right are exactly the same). This symmetry, however, does not exist for up-down mirrored nodes because of the transmitting antenna pattern, which favors up. For this reason, all nodes on the right half of the map are omitted from the results.

The received power at all stations is calculated by adding the complex field magnitude of rays that cross the stations. Based on the direction of arrival (DOA) of each ray and orientation of the receiving antenna, the antenna gain is added to the field intensity. At each receiving station, received power is calculated for two different antenna orientations: one with the main beam pointing toward the transmitting antenna (or toward the angle of incidence of the strongest ray, which is the diffracted ray for stations without a clear LOS toward the TX) and the other with the main beam pointing away from the TX. For comparison, FS and FS plus ground (FSG) reflection predictions are also calculated and displayed along with the simulation results.

All received power calculations are carried out on a 9-point window around the RX, that is, on a 3×3 grid centered at the receiving node with a distance of 0.5 m between points.

III. Simulation Results and Discussion

Figures 6(a) and 6(b) show the results of our simulation in LOS stations with RX antennas pointed toward and away from the TX. FS and FSG reflection predictions are displayed as well for comparison. All results are normalized to the desired signal level (signal level at the southward link of node 32). In the FS scenario, it is assumed that there are no obstructions present in the environment, with the FSG reflection scenario taking into account the presence of ground reflected components in an otherwise empty environment. Figures 6(c) and 6(d) show the same results for non-LOS (NLOS) stations.

It is clear from the results that LOS stations show better agreement with the FS and FSG predictions than NLOS due to the presence of the LOS component. FS and FSG predictions significantly overestimate received power in NLOS stations. At NLOS stations, the strong FS component is blocked by buildings and, seeing as consecutive reflections cannot propagate into crossing streets far enough to get to NLOS

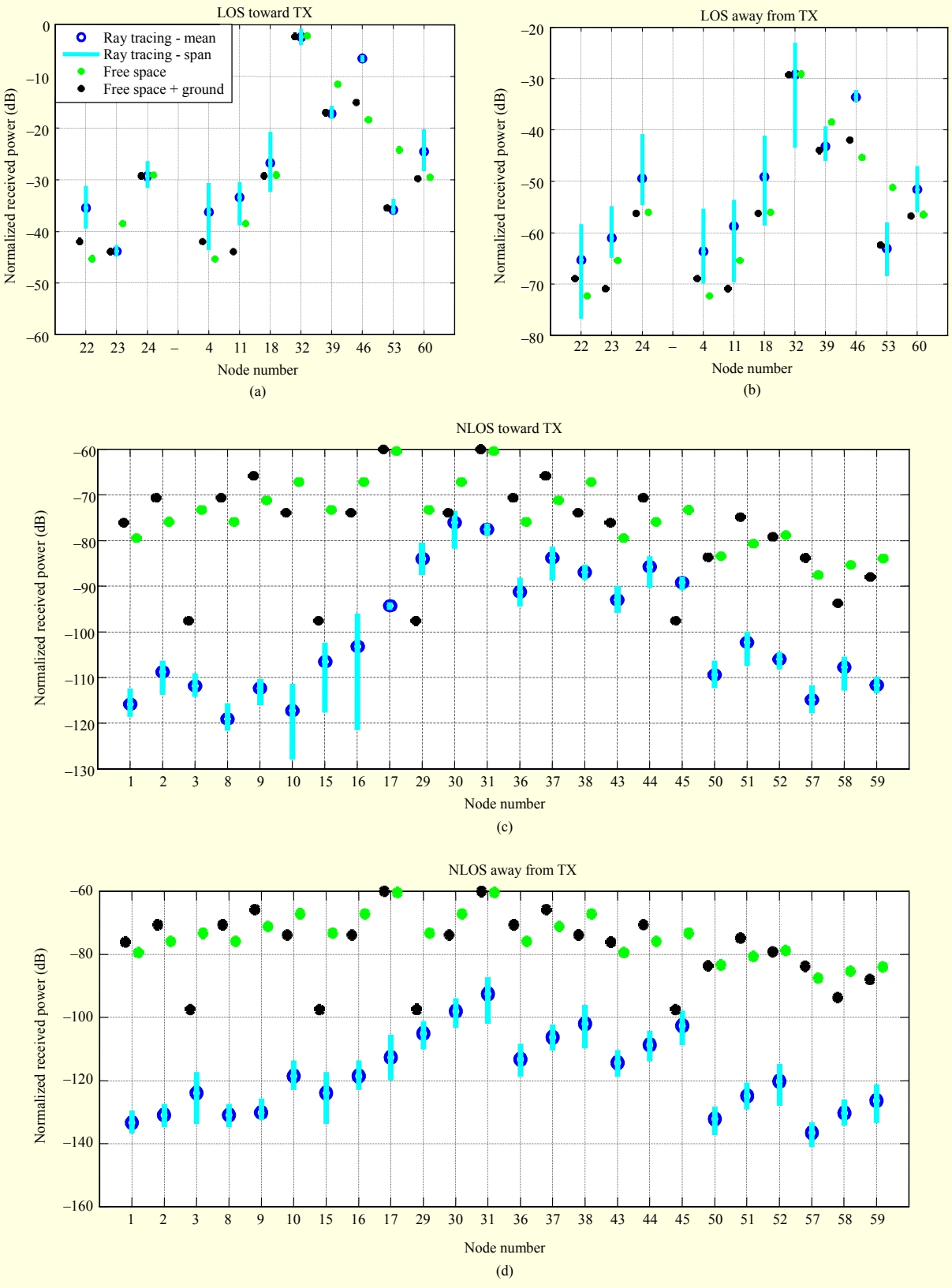

Fig. 6. Results of simulation, FS, and FSG reflection predictions for (a) LOS nodes with antennas pointed toward strongest incident ray, (b) LOS nodes with antennas pointed away from strongest incident ray, (c) NLOS nodes with antennas pointed toward strongest incident ray, and (d) NLOS nodes with antennas pointed away from strongest incident ray.

stations, diffraction is the main mechanism of penetration toward NLOS stations. The sizable gap between FS/FSG and ray tracing simulations is basically the result of a severe diffraction loss suffered by these components. This loss can be roughly calculated by

$$L_{\text{ex}} = \frac{d_1 + d_2}{d_1 d_2} \frac{\lambda}{4n^2} \sum \cot(\gamma_i), \quad (1)$$

$$\gamma_i = \frac{\pi \pm (\varphi_1 \pm \varphi_2)}{2n}, \quad n = 2 - \theta_c / \pi, \; i = 1, 2, 3, 4,$$

where d_1 and d_2 respectively represent the distances of the TX and RX from the diffraction point and λ is the wavelength; the other parameters are defined in Fig. 7 [33].

At some points, however, this gap seems to shrink. This is due to antenna orientation and directivity at transmitting and receiving stations. According to (1), excess diffraction loss is about 60 dB to 70 dB. Figure 6(d) shows that the difference between FS and ray tracing is about this much for stations 1, 2, 3, 8, 9, and 10. However, in the rest of the stations, the main beam gain of the TX antenna is added to the ray, decreasing the gap between FS and ray tracing. As shown in Fig. 6(c), when the RX antenna is pointed in the direction of the incoming ray, this gap is further decreased and practically vanishes at the nearer nodes. This shows that environment geometry affects the channel response in many ways. Buildings block the LOS for many links, but they also introduce a wave guiding effect, which may result in stronger rays propagating into unexpected areas.

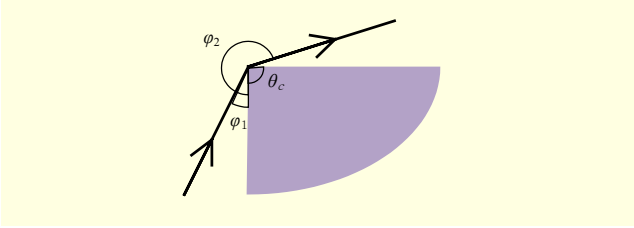

Fig. 7. Diffraction geometry and parameters.

By taking into account the environmental obstacles and antenna orientations, the excess loss calculated in (1) and antenna gains in the direction of the diffraction path (which differ from the FS path considered before) are added to the FS predictions, resulting in better agreement between these modified predictions and the simulation results. These results are shown in Fig. 8.

In the simplified map that we consider, LOS stations are located on the same street as the transmitting node. In these links, rays that deliver power include the LOS ray and single or multiple reflections from the ground and walls of the street. Reception of many reflected rays (with the same order of power) leads to an increase in the variation of received power. We expect that the farther away the TX is from the station, the more significant the decrease in signal levels. However, as shown in Fig. 6(a), at node 46, for instance, a combination of reflected components can increase signal levels to several decibels above LOS predictions. This means that more nodes can be considerably affected by the interference of the designated TX. In other words, the guiding behavior of the street calls for the provision of a higher margin when predicting the signal-to-noise plus interference ratio (SNIR) for network design.

NLOS points may also be subject to multipath fading. In our modified FS model, we consider a single diffracted ray. However, in general, several diffraction points (with similar geometry and distances) may exist between the TX and RX,

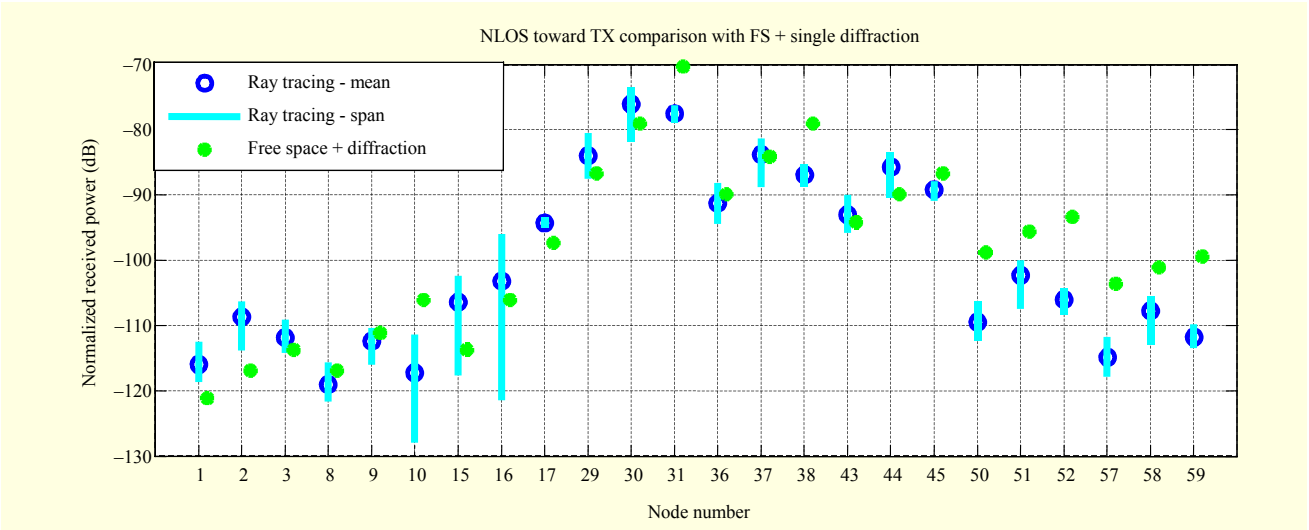

Fig. 8. Comparison of ray tracing results for NLOS nodes with modified FS with diffraction loss predictions.

and each diffracted component may also have corresponding reflected components.

Figure 9 shows the available diffraction points in our simple scenario. The corners represented by a light dot in the figure diffract rays coming from the main beam, and the corners represented by a dark dot in the figure diffract rays from the sidelobes of the transmitting antenna. How each ray is picked up at the RX depends on the orientation of the receiving antenna. The interaction of these rays and their reflections at the RX cause variations in the received power. Of course, received components at NLOS stations are normally quite weak, and it is unlikely that the combination of several of these rays would disrupt the link quality or SNIR.

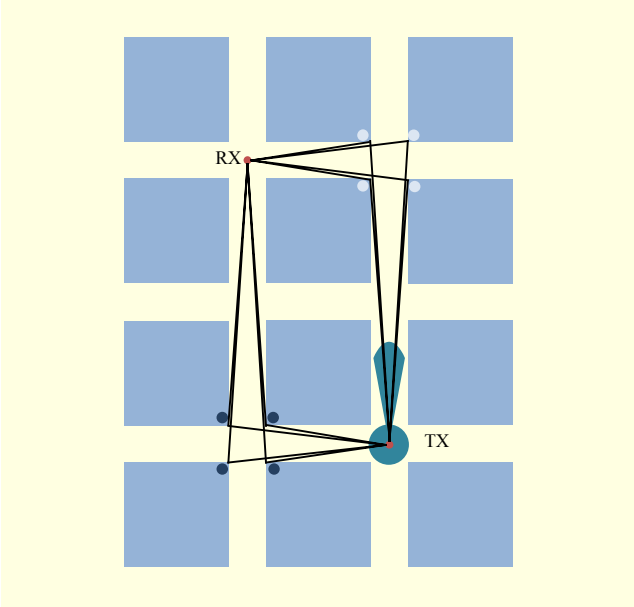

Fig. 9. Different available diffraction paths.

1. Channel Description for LOS Links

The received signal at LOS RXs is the sum of a number of components or rays with the same order of power and random relative phase. The number of these rays and their power determine the statistical description of received signal strength. The power a ray produces at the RX is mostly dependent upon its angle of departure and DOA. Rays that are emitted from the main beam of the TX antenna are at least 27 dB stronger than rays emitted from a sidelobe. The same holds true for rays received from the main beam of the receiving antenna. The number of rays emitted from and received by the main beam depends on the beamwidth of the TX and RX antennas, the street width (W), and the link length (distance between TX and RX stations, denoted by L).

Assuming a ray is reflected N times, the distance of the first incidence on the wall equals $L/2N$. If this point falls at the part of the wall illuminated by the main beam of the antenna, the ray is emitted from the main beam. The minimum distance on the wall that is illuminated by the main beam (as shown in Fig. 10) is

$$\frac{W}{2}\cot\left(\frac{\theta_{\mathrm{BW}}}{2}\right).$$

Therefore, a ray reflected N times is emitted from the main lobe if

$$\frac{L}{2N} \geq \frac{W}{2}\cot\left(\frac{\theta_{\mathrm{BW}}}{2}\right). \tag{2}$$

The largest N that satisfies this requirement is

$$N = \left\lfloor \frac{L}{W}\tan\left(\frac{\theta_{\mathrm{BW}}}{2}\right) \right\rfloor. \tag{3}$$

Therefore, the number of reflected components emitted from

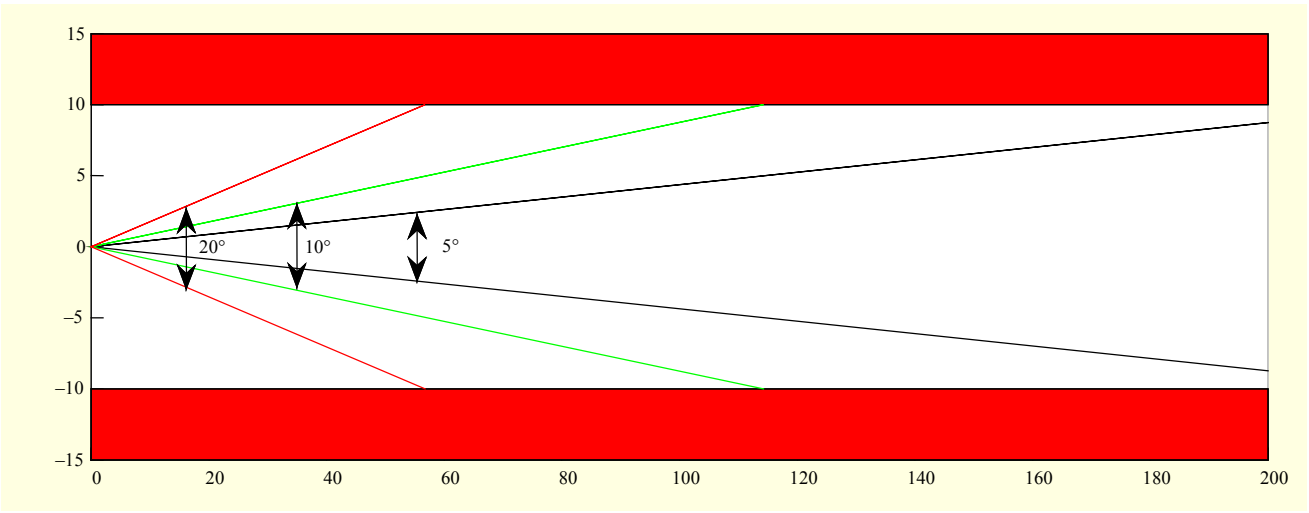

Fig. 10. Main beam illumination distance on street walls for different antenna beamwidths.

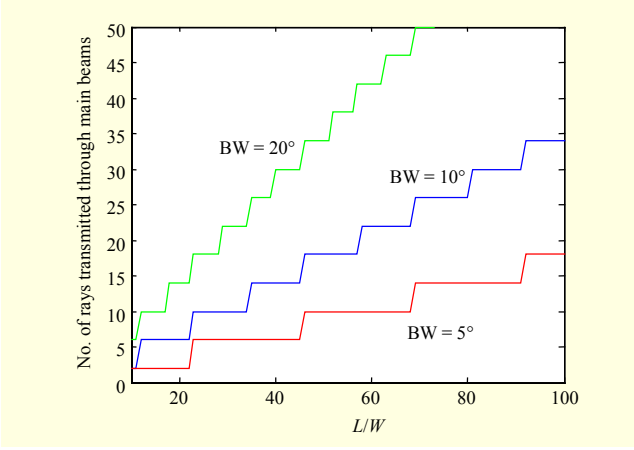

Fig. 11. Number of main beam rays as function of distance to width ratio for different antenna beamwidths.

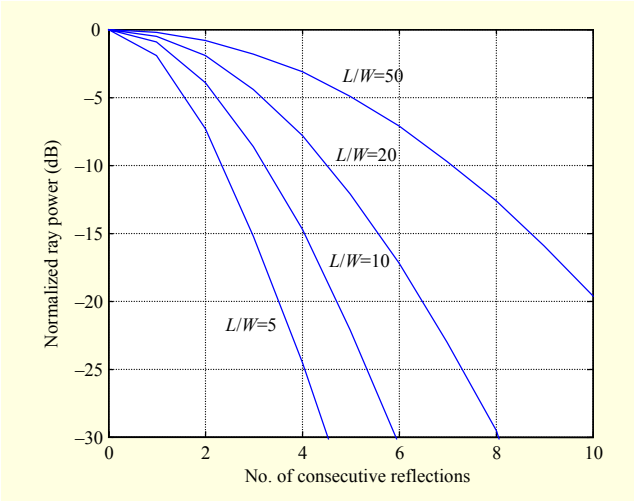

Fig. 12. Normalized ray intensity as a function of number of consecutive reflections for different L to W ratios.

the main lobe is $2N$ (each number of reflections occurs twice, once starting with the left wall and again with the right wall). Each component has a reflection from the ground as well, and we also have the LOS component and its ground reflection; so, $n = 4N+2$ rays emitted from the main beam reach the RX. In a scenario in which antennas are located at equal distances from the right and left walls, due to symmetry, all rays emitted from the main lobe are picked up from the main lobe, granted that the receiving antenna is pointed in the direction of the TX. In a scenario with different assumptions for antennas and placement of nodes, these conclusions would differ; however, qualitatively, the dependence of n on L, W, and θ_{BW} would be the same.

Figure 11 shows the number of rays transmitted from and to the main beam as a function of distance-to-street-width ratio for various antenna beamwidths. Of course, not all of these rays contain the same amount of power. When N (number of reflections) becomes large, so does the grazing angle of reflections and therefore the overall attenuation caused by reflections. Figure 12 shows the normalized ray power as a function of the number of consecutive reflections for different L/W ratios.

In the absence of main beam rays, that is, rays that are either emitted or received from the main beam, many components with similar order signal power reach the RX, increasing the variation in signal strength. This increase in variation is clear from Figs. 6(b) and 6(d), in which RXs pointing away from the TX and placed behind the main beam of the transmitting antenna show much higher variation in signal strength than links with the beam of at least one end pointed toward the link.

When considering reception (and not interference), received power is not the only significant factor. Link quality is also affected by the difference in time delay of received components, which limits the bitrate of a link by controlling inter-symbol interference. In addition, correlation length can also be an important characteristic for links that use MIMO or spatial diversity. Both of these parameters are evaluated in the context of the described scenario for LOS links.

2. Time Delay Difference of Rays

The time difference between receptions of different rays is proportional to their propagation distance. In a street of width W, with TX and RX antennas with beamwidth θ_{BW}, a link with length of L will have n components, where n is calculated using the equations described previously.

The shortest path is the LOS with length L (assuming TX and RX antennas are at equal height, h). The longest path, which falls inside the main beams of both antennas, undergoes N reflections off street walls and one off the ground. The length of this path is

$$\sqrt{L^2+(NW)^2+(2h)^2} \approx L\left(1+\frac{1}{2}\left(\frac{NW}{L}\right)^2+2\left(\frac{h}{L}\right)^2\right).$$

Therefore, the distance difference between the shortest and longest paths is

$$\Delta L = \frac{1}{2}\frac{(NW)^2}{L}+2\frac{h^2}{L}. \quad (4)$$

From here, the maximum time delay between components can be calculated by

$$\Delta\tau = \Delta L / c,$$

where c is the speed of propagation. For instance, for the map used in this simulation with $W = 20$ m, $L = 200$ m, and $h = 3$ m

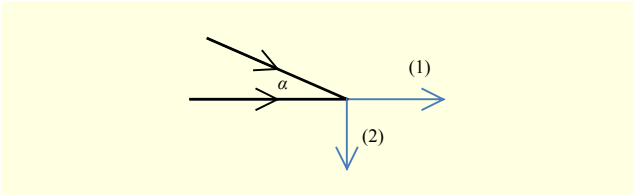

Fig. 13. Angular span of incoming rays and directions (1) and (2) for calculating correlation length.

for a beamwidth that allows $N = 2$, we have

$$\Delta L = \frac{1}{2}\frac{(2.20)^2}{200} + 2\frac{3^2}{200} = 4.09\,\text{m},$$

which corresponds to a time delay of $\Delta\tau = \Delta L / c = 13.6$ ns between the earliest and latest received rays.

3. Correlation Length

One factor that is affected by the DOA of rays at the RX is the correlation length. In a propagation environment in which rays arrive at the RX from all directions, the correlation length of the channel is in the same order of magnitude as a wavelength. However, when the DOA is limited to a small angular span, the correlation length increases. When the wave vector of incoming rays is similar, moving the RX in a certain direction induces similar amounts of phase change in all the received components, keeping the result of their overall interaction almost unchanged. Assuming all received rays fall within an angular span of α, moving the RX L meters in one of the directions shown in Fig. 13 results in a maximum relative phase change of

$$|\Delta\theta_1| = |Lk - Lk\cos\alpha| = Lk(1-\cos\alpha),$$
$$|\Delta\theta_2| = |0 - Lk\cos(\pi/2 - \alpha)| = Lk|\sin\alpha|.$$

Therefore, assuming a maximum relative phase turn of $\pi/2$ is required for loss of correlation; the correlation length in each direction is expected to be

$$CL_1 = \frac{\lambda}{4(1-\cos\alpha)},$$
$$CL_2 = \frac{\lambda}{4|\sin\alpha|},$$

which, for small α, can be several orders of magnitude greater than λ.

IV. Conclusion and Future Work

We observed that blockage caused by buildings affects the channel response in different areas in a variety of ways. In NLOS areas, blockage of the LOS component results in reflection and diffraction when delivering signal power to RXs. Due to the length of the streets, it takes many consecutive reflections for a ray to propagate through the LOS street, reflect around a corner, and continue traveling toward the NLOS receiving node. These reflections have small incident angles and can be attenuated severely by roughness. In fact, if diffraction is not addressed, rays only reach a few nearby NLOS nodes with a significant power level. Limited penetration of reflected rays into crossing streets causes diffraction to be the main conveyer of signals to NLOS areas, resulting in a substantial decrease in power levels. Both blockage caused by buildings and antenna orientation must be taken into account to accurately predict signal levels in NLOS stations.

In LOS areas, however, the average received power does not differ greatly from FS predictions; yet, street surfaces introduce several reflected components as well. The combination of these components can result in variations in the received signal power, which may result in overestimation of desired signals or underestimation of interference from LOS TXs in some cases; especially in faraway nodes where more reflections come into the main beam zone, we have more components and therefore a higher standard deviation. If not considered appropriately, this higher variation can result in interference levels exceeding the margin and thus damage the link quality. In other words, the wave guiding effect of street surfaces brings about the need to reconsider SNIR margins.

Other channel characteristics, such as time delay and correlation length at LOS receiving points, were also evaluated. It was observed that because of the small angular span of incident rays, signal levels of nearby points are strongly correlated and the correlation length of the channel is much greater than the wavelength.

In the continuation of this work, similar simulations will be carried out in different environment models. We will apply the work presented herein to a real city environment to assess the conclusions.

References

[1] AIRLINX, GigaLink 6221/6421/6451. http://www.airlinx.com/products.cfm/product/1-20-671.htm

[2] S. Alalusi and R. Brodersen, "A 60 GHz Phased Array in CMOS," *Proc. IEEE CICC*, Sept. 2006, pp. 393-396.

[3] D. Liu and R. Sirdeshmukh, "A Patch Array Antenna for 60 GHz Package Applications," *Proc. IEEE AP-S Symp.*, 2008, pp. 1-4.

[4] C.-C. Chong et al., "Millimeter-Wave Wireless Communication Systems: Theory and Applications," *EURASIP J. Wireless Commun. Netw.*, 2007.

[5] T. Tjelta et al., "An Evaluation of Future Mobile Networks

Backhaul Options," *5th Int. Conf. Wireless Mobile Commun.*, 2009.

[6] T. Tjelta, "Gigabit Radio Links for Flexible and Efficient Broadband Mobile Backhaul Networks," *Telektronikk*.

[7] S.M. Das et al., "DMesh: Incorporating Practical Directional Antennas in Multichannel Wireless Mesh Networks," *IEEE J. Sel. Areas Commun. Special Issue Multi-hop Wireless Mesh Netw.*, vol. 24, no. 11, 2006, pp. 2028-2039.

[8] G. Li et al., "Opportunities and Challenges for Mesh Networks Using Directional Antennas," *Proc. IEEE Workshop Wireless Mesh Netw.*, *SECON*, 2005.

[9] Y.-B. Ko, J.M. Choi, and N.H. Vaidya, "MAC Protocols Using Directional Antennas in IEEE 802.11 Based Ad Hoc Networks," *Wireless Commun. Mobile Comput.*, vol. 8, no. 6, 2007, pp. 783-795.

[10] R.R. Choudhury et al., "On Designing MAC Protocols for Wireless Networks Using Directional Antennas," *IEEE Trans. Mob. Comp.*, vol. 5, no. 5, 2006, pp. 477-491.

[11] R. Ramanathan et al., "Ad Hoc Networking with Directional Antennas: A Complete System Solution," *IEEE J. Sel. Areas Commun.*, vol. 23, no. 3, Mar. 2005, pp. 496-506.

[12] Z. Huang and C.-C. Shen, "A Comparison Study of Omnidirectional and Directional MAC Protocols for ad hoc Networks," *Proc. IEEE Globecom*, 2002.

[13] A. Nasipuri et al., "A MAC Protocol for Mobile Ad Hoc Networks Using Directional Antennas," *Proc. IEEE WCNC*, vol. 3, 2000, pp. 1214-1219.

[14] L. Bao and J. Garcia-Luna-Aceves, "Transmission Scheduling in Ad Hoc Networks with Directional Antennas," *Proc. Mobicom*, 2002.

[15] V. Ramamurthi et al., "Link Scheduling and Power Control in Wireless Mesh Networks with Directional Antennas," *IEEE Int. Conf. Commun.*, 2008, pp. 4835-4839.

[16] P. Smulders, "Statistical Characterization of 60 GHz Indoor Radio Channels," *IEEE Trans. Antennas Propag.*, vol. 57, no. 10, 2009, pp. 2820-2829.

[17] T. Manabe, Y. Miura, and T. Ihara, "Effects of Antenna Directivity and Polarization on Indoor Multipath Propagation Characteristics at 60 GHz," *IEEE J. Sel. Areas Commun.*, vol. 14, no. 3, 1996, pp. 441-448.

[18] M. Park and P. Gopalakrishnan, "Analysis on Spatial Reuse, Interference, and MAC Layer Interference Mitigation Schemes in 60 GHz Wireless Networks," *IEEE Int. Conf. Ultra-Wideband*, 2009, pp. 1-5.

[19] H. Xu, V. Kukshya, and T.S. Rappaport, "Spatial and Temporal Characteristics of 60 GHz Indoor Channels," *IEEE J. Sel. Areas Commun.*, vol. 20, no. 3, 2002, pp. 620-630.

[20] S. Singh et al., "Blockage and Directivity in 60 GHz Wireless Personal Area Networks: From Cross-Layer Model to Multihop MAC Design," *IEEE J. Sel. Areas Commun.*, vol. 27, no. 8, Oct. 2009.

[21] N. Moraitis and P. Constantinou, "Indoor Channel Measurements and Characterization at 60 GHz for Wireless Local Area Network Applications," *IEEE Trans. Antennas Propag.*, vol. 52, no. 12, 2004.

[22] Z. Fan, "Wireless Networking with Directional Antennas for 60 GHz Systems," *14th European Wireless Conf.*, June 2008.

[23] A. Maltsev et al., "Statistical Channel Model for 60 GHz WLAN Systems in Conference Room Environment," *Proc. 4th European Conf. Antennas Propag.*, 2010.

[24] S. Singh, R. Mudumbai, and U. Madhow, "Distributed Coordination with Deaf Neighbors: Efficient Medium Access for 60 GHz Mesh Networks," *Proc. IEEE INFOCOM*, 2010, pp. 1-9.

[25] R.C. Daniels and R.W. Heath, "60 GHz Wireless Communications: Emerging Requirements and Design Recommendations," *IEEE Veh. Technol. Mag.*, vol. 2, no. 3, 2007, pp. 41-50.

[26] S. Singh, R. Mudumbai, and U. Madhow, "Interference Analysis for Highly Directional 60 GHz Mesh Networks: The Case for Rethinking Medium Access Control," *IEEE/ACM Trans. Netw.*, vol. 19, no. 5, Oct. 2011, pp. 1513-1527.

[27] J.H. Whitteker, "Measurements of Path Loss at 910 MHz for Proposed Microcell Urban Mobile Systems," *IEEE Trans. Veh. Technol.*, vol. 37, 1988, pp. 125-129.

[28] M.E. Rasekh, *Statistical-Empirical Modeling of Millimeter Wave Propagation (at 60 GHz) for Wireless Communications*, master's thesis, School of Electrical Engineering, Sharif University of Technology, 2009.

[29] A.M. Hammoudeh, M. Garcia Sanchez, and E. Grindrod, "Experimental Analysis of Propagation at 62 GHz in Suburban Mobile Radio Microcells," *IEEE Trans. Veh. Technol.*, vol. 48, no. 2, 1999, pp. 576-588.

[30] M. Atamanesh and F. Farzaneh, "A Proposed Equivalent Channel Power Delay Profile for a Millimeter Wave Wireless OFDM System and Optimum Guard Interval Evaluation in a Built-Up Area Propagation Scenario," *Wireless Personal Commun.*, 2012.

[31] M.E. Rasekh, F. Farzaneh, and A.A. Shishegar, "A Street Canyon Approximation Model for the 60 GHz Propagation Channel in an Urban Environment with Rough Surfaces," *5th Int. Symp. Telecommun.*, 2010.

[32] J.B. Keller, "Geometrical Theory of Diffraction," *J. Opt. Soc. America*, vol. 52, 1962, pp. 116-130.

[33] H. Wang and T.S. Rappaport, "A Parametric Formulation of the UTD Diffraction Coefficients for a Dielectric Wedge," *IEEE Antennas Wireless Propag. Lett.*, vol. 4, 2005, pp. 253-257.

Maryam Eslami Rasekh was born in Isfahan, Iran, in 1985. She received her BSc in electrical engineering from Isfahan University of Technology, Iran, in 2007 and her MSc from Sharif University of Technology, Tehran, Iran, in 2009. She is currently working toward a PhD degree in the Department of Electrical Engineering of Sharif University of Technology. Her research areas include wave propagation and channel modeling and wireless networking.

Forouhar Farzaneh was born in Teheran, Iran, in 1957. He received his B.Sc. in electrical engineering from the University of Shiraz, Iran, in 1980, his M.Sc. from ENST-Paris in 1981, and his DEA and doctorate from the University of Limoges, France, in 1982 and 1985, respectively. He was with Tehran Polytechnic from 1985 to 1989. Since 1989, he has been with the Department of Electrical Engineering, Sharif University of Technology, where he is a professor. He was a co-recipient of the Microwave Prize — European Microwave Conference in 1985 and a recipient of the Maxwell Premium of IEE in 2001.